Supplementary Information

Anchoring Ru Single-Atom on MXene Achieves Dual-Enzyme Activities for Mild Photothermal Augmented Nanocatalytic Therapy

Wenzhuo Wang,[a,‡] Yanlin Zhu,[a,‡] Lili Feng,[a,] Ruoxi Zhao,[a] Chenghao Yu,[a] Yaoyu Hu,[a] Zhen Hu,[a] Bin Liu,[a] Lei Zhong,[b] and Piaoping Yang[a,]**

[a] Key Laboratory of Superlight Materials and Surface Technology, College of Materials Science and Chemical Engineering, Ministry of Education, Harbin Engineering University, Harbin 150001, P. R. China

[b] Department of Breast Surgery, the Second Affiliated Hospital of Harbin Medical University, Harbin 150086, P. R. China

* E-mail: fenglili@hrbeu.edu.cn; yangpiaoping@hrbeu.edu.cn

‡ These authors contributed equally

Experimental Section

Materials. Ti_3AlC_2 (powder, 200-meshes) was purchased from Foshan Xinxi Technology Co., Ltd., hydrofluoric acid (HF), lithium fluoride (LiF), hydrochloric acid (HCl), ruthenium (III) chloride ($RuCl_3$), potassium bromide (KBr), o-phenylenediamine (OPD), and 3,3′,5,5′-tetramethyl-benzidine (TMB) were achieved from Aladdin (Shanghai, China). 5,5-dimethyl-pyrroline-N-oxide (DMPO), methylthiazolyldiphenyl-tetrazolium bromide (MTT), 4′,6-diamidino-2-phenylindole (DAPI), methylene blue, Calcein-AM, and propidium iodide (PI) were obtained from Sigma-Aldrich. 2',7'-dichloro fluorescent yellow diacetate (DCFH-DA) was purchased from Thermo Fisher Scientific. Hematoxylin and eosin staining (H&E) and terminal deoxynucleotidyl transferase-mediated dUTP-biotin nick end labeling (TUNEL) detection kit were bought from Dalian Meilun Biotechnology Co, Ltd. Deionized water was utilized throughout the whole experiment. All the chemical agents were utilized as received without further purification.

Instruments. Transmission electron microscopy (TEM) was used to observe the morphology of the prepared nanomaterials by the FEI Tecnai T20 transmission electron microscope. Aberration-corrected high-angle annular dark-field scanning transmission electron microscopy (AC HAADF-STEM). The X-ray photoelectron spectroscopy (XPS) spectrum analysis was performed using the Thermo Fisher Scientific ESCALAB 250XI. X-ray diffraction (XRD) pattern of sample was examined with a Rigaku D/max-TTR-III diffractometer using Cu-Ka radiation (λ = 0.15405 nm) at 40 kV and 40 mA. Atomic force microscope (AFM) measurement was conducted on the Veeco DI Nanoscope Multi-Mode V system. The dynamic light scattering (DLS) and zeta potential measurement of various samples were carried out using a Malvern Zeta sizer Nan Nano ZS90. Fourier transform infrared (FTIR) spectra were collected by using a Thermo Nicolet Nexus 670 ATR-IR spectrometer. The electron paramagnetic resonance (ESR) spectra were measured by an electron paramagnetic resonance spectrometer (JEOL-FA200, JEOL, Japan). The temperature change of

different samples was conducted using an infrared thermal imaging instrument (FLIR A325SC camera). A confocal laser scanning microscope (CLSM, Leica TCS SP8) was utilized to observe the fluorescence image. The content of Ti was detected by inductively coupled plasma mass spectroscopy (ICP-OES, Agilent 725, Agilent Technologies, US). Photothermal images were recorded using an Inf Rec R300SR-HD infrared thermal imager. The photoacoustic (PA) images were obtained using the Vevo LAZR-X system.

Preparation of $Ti_3C_2T_x$. 2D $Ti_3C_2T_x$ nanosheets were prepared based on a previously published method with slight modifications. First, LiF (1.5 g) was added into HCl (18 mL, 12 M) and HF (2 mL, 49%) mixture solution. Next, Ti_3AlC_2 powders (1 g) were slowly added and stirred vigorously for 30 min at 24 ℃. Then, the temperature of the mixture was set to 48 ℃ and held for 48 h. After the reaction was completed, the mixture was centrifuged and rinsed using deionized water for eight times. After the completion of the reaction, the mixture was centrifuged and washed with HCl for five times. HCl was then washed away using deionized water by centrifugation, until the pH was closed to neutral. Finally, the mixture was treated with ultrasound for several times. The colloidal dispersion of $Ti_3C_2T_x$ nanosheets was achieved by centrifugation. At last, the $Ti_3C_2T_x$ were dispersed in water and stored at 4℃ for follow-up experiment.

Preparation of Ru-$Ti_3C_2T_x$. Typically, $Ti_3C_2T_x$ (20 mg) and $RuCl_3$ (20 mg) were added into NaOH aqueous solution (40 mL, 0.4 mM), and thoroughly stirred at 25 ℃ without light for 12 h. The mixture solution was collected by centrifugation and followed by rinsed with deionized water for three times, after the reaction was completed. At last, the Ru-$Ti_3C_2T_x$ nanosheets were dissolved in water and stored in the refrigerator for follow-up experiment.

Preparation of Ru-$Ti_3C_2T_x$-PEG nanozymes. In the surface modification process of nanosheets, NH_2-mPEG (10 mg) was slowly added into deionized water (10 mL) upon ultrasonic treatment with a sub-zero water bath. Then, the obtained NH_2-mPEG were slowly added into Ru-$Ti_3C_2T_x$ solution (5 mg) with

vigorously stirred. After stirring for about 24 h, the obtained mixture was centrifuged and washed with deionized water, and the Ru-$Ti_3C_2T_x$-PEG was collected. At last, the Ru-$Ti_3C_2T_x$-PEG nanozymes were dispersed in deionized water and stored in the refrigerator for follow-up experiment.

The CAT-like activity of Ru-$Ti_3C_2T_x$-PEG. The CAT-like activity of Ru-$Ti_3C_2T_x$-PEG was measured to evaluate the production of dissolved oxygen, and a dissolved oxygen meter was used for this experiment. Ru-$Ti_3C_2T_x$-PEG and 10 mL phosphate buffer solution (PBS) were mixed entirely with the final concentrations of 100, 200, 300, and 400 μg mL^{-1}, respectively. Then, H_2O_2 was dripped into the above solution with the final concentration 200 μM. The O_2 generation was recorded by the dissolved oxygen meter every 10 s.

The degradation of methylene blue (MB). At first, Ru-$Ti_3C_2T_x$-PEG nanocomposites were dispersed in MB aqueous solution with the final concentration of 200 μg mL^{-1}. Next, H_2O_2 was dripped into the above solution with the final concentration was 50 μM. By centrifugation to remove the influence of Ru-$Ti_3C_2T_x$-PEG, the absorption spectrum of the supernatant was obtained by UV−vis spectrophotometer after different time intervals (0, 5, 10, 20, and 30 min). Under the same conditions, the influence of 808 nm laser on the degradation of MB was further performed.

Peroxidase-like (POD-like) activity and kinetic analysis of Ru-$Ti_3C_2T_x$-PEG. First, the POD enzyme activity of Ru-$Ti_3C_2T_x$-PEG in the presence of H_2O_2 was evaluated, OPD and TMB were selected as indicators. The UV−vis spectrophotometer was used to measure the absorbance of the supernatant, while simultaneously the color alteration of the solution was recorded. Under the same conditions, the effects of both sample concentration and NIR laser on the enzyme activity were measured.

***In vitro* cell viability assessment.** To evaluate the biocompatibility cytotoxicity of Ru-$Ti_3C_2T_x$-PEG, L929

cells (L929 fibroblast cell line) and CT26 cells (CT26 mouse breast cancer cells) were examined using standard thiazole tetrazolium (MTT) assay. CT26 cells were first inoculated in a 96-well plate, and then treated with different formulations, including G1: Control, G2: Laser, G3: $Ti_3C_2T_x$-PEG, G4: Ru-$Ti_3C_2T_x$-PEG, G5: $Ti_3C_2T_x$-PEG + Laser, G6: Ru-$Ti_3C_2T_x$-PEG + Laser. After 12 h of cultivation, PBS was used to wash the cells, then 20 μL of MTT solution (5 mg mL^{-1}) was dripped addition in each well. 150 μL of DMSO was added immediately after 4 h, the absorbance at 490 nm was detected for calculating the cell viability. Similarly, L929 cells were treated with $Ti_3C_2T_x$-PEG and Ru-$Ti_3C_2T_x$-PEG in different concentrations for 24 h, and other experimental procedures are consistent with cytotoxicity tests.

Cellular uptake assay. CT26 cells with the density of 1×10^5 were planted into the six-well plate and incubated overnight. FITC-labeled Ru-$Ti_3C_2T_x$-PEG was added and incubated for different periods. Then, the CT26 cells were cleaned with PBS, and DAPI was selected to stain the cell nuclei for a duration of 15 min. The cells were collected and analyzed by CLSM to observe the phagocytosis.

Intracellular ROS evaluation. CT26 cells were inoculated on six-well plate and fostered overnight. The cells were treated with various groups, containing G1: Control, G2: Laser, G3: $Ti_3C_2T_x$-PEG, G4: Ru-$Ti_3C_2T_x$-PEG, G5: $Ti_3C_2T_x$-PEG + Laser, G6: Ru-$Ti_3C_2T_x$-PEG + Laser. The concentration of $Ti_3C_2T_x$-PEG and Ru-$Ti_3C_2T_x$-PEG was 200 μg mL^{-1}. After 4 h of incubation, the cells were cleaned up and dark stained with DCFH-DA solution for 20 min. Then the cells were cleaned with PBS, and then DAPI was selected to stain the cell nuclei for 15 min. Then, the cells were further washed and intracellular fluorescence intensity was observed by CLSM. Another group of similarly treated cells were digested and washed with chymotrypsin, analyzed by a flow cytometry and the fluorescence intensity was recorded to quantify the production of ROS by flow cytometry in a more precise manner.

Cytoskeleton staining. CT26 cells were plated in six-well plate with the density of 1×10^5 and cultured for

24 h in a CO_2 incubator. The cells were treated with Control, Laser, $Ti_3C_2T_x$-PEG, Ru-$Ti_3C_2T_x$-PEG, $Ti_3C_2T_x$-PEG + Laser, and Ru-$Ti_3C_2T_x$-PEG + Laser, respectively. After 4 h of incubation, the nucleus and F-actin filaments were stained with DAPI (15 min) and Actin Red (20 min), respectively. Subsequently, the cells were collected and the cell morphology was observed by CLSM.

Intracellular oxygen production. Oxygen production was analyzed using $[Ru(dpp)_3]^{2+}Cl_2$ as a detection probe. CT26 cells were incubated on a six-well plate for 24 h. After that, fresh medium enriched with Ru-$Ti_3C_2T_x$-PEG (200 μg mL^{-1}) was introduced and co-cultured for 4 h, and $[Ru(dpp)_3]^{2+}Cl_2$ dyeing reagent with the concentration of 10 μM was added and the mixture was incubated in the dark for 20 min. The cells were rinsed with PBS, and subsequently stained with DAPI for 15 min to visualize the cell nuclei. Finally, the cells were washed and CLSM was performed to analyze the fluorescence intensity.

Mitochondrial membrane potential assay. The whole layer of CT26 cells was covered on the six-well plate. The cells were treated under different conditions, including Control, Laser, $Ti_3C_2T_x$-PEG, Ru-$Ti_3C_2T_x$-PEG, $Ti_3C_2T_x$-PEG + Laser, and Ru-$Ti_3C_2T_x$-PEG + Laser. The concentration of $Ti_3C_2T_x$-PEG and Ru-$Ti_3C_2T_x$-PEG was 200 μg mL^{-1}. After 4 h of incubation, the cells were stained with the JC-1 assay kit according to the instructions. Subsequently, the cells were stained with DAPI for 15 min to visualize the cell nuclei. Finally, the cells were analyzed under CLSM.

Living/dead cells staining. The Calcein-AM and propidium iodide were used to distinguish the living and dead cells. The whole layer of CT26 cells were covered on the six-well plate and incubated with $Ti_3C_2T_x$-PEG or Ru-$Ti_3C_2T_x$-PEG at the same concentration of $Ti_3C_2T_x$ (200 μg mL^{-1}). For the laser irradiation groups, the treatment protocol remained identical to the aforementioned process, with an additional step of being irradiated by an 808 nm laser for a duration for 5 min. Afterwards, Calcein-AM and PI were added and incubated for 30 min. The cells were rinsed with PBS and observed by CLSM.

Apoptosis detection assay. Quantitative analysis of apoptosis-mediated cell death was performed using a flow cytometer. The whole layer of CT26 cells were covered on the six-well plate and incubated with $Ti_3C_2T_x$-PEG or Ru-$Ti_3C_2T_x$-PEG with the same concentration of $Ti_3C_2T_x$ (200 μg mL^{-1}). For the laser irradiation group, the cells were exposed to an 808 nm laser with the power density of 0.8 W cm^{-2} for a duration of 5 min. After the cells continued to incubate for 4 h, and all cells were digested with trypsin, washed, and collected in the separate tubes. After removing the residual nanozymes, 5 μL of Annexin V-FITC was introduced into each well and allowed to incubate in darkness for 15 min. Subsequently, 10 μL of PI was added, and the samples were kept under identical experimental conditions for another 5 min. Ultimately, the cytotoxicity of each group was evaluated through flow cytometry analysis.

Tumor mouse model. The female BALB/c mice with the average body weight of about 15 g at the age of 4 weeks were purchased. All the mice were reared in optimal conditions, provided with sterile food and water. The CT26 cells (2×10^6) dispersed in 100 μL PBS were subcutaneously injected into the right hind limb of each BALB/c mouse to establish a tumor model. The *in vivo* antitumor treatment efficacy evaluation was performed when the tumor volume grew to about 60 mm^3.

***In vitro* and *in vivo* PA imaging.** Firstly, the polyethylene capillaries were filled with Ru-$Ti_3C_2T_x$-PEG aqueous solution at various concentrations, and then added with the coupling gel to perform *in vitro* PA imaging. To evaluate the *in vivo* PA imaging effect, Ru-$Ti_3C_2T_x$-PEG solution with the dose of 10 mg kg^{-1} was injected intravenously into CT26 tumor-bearing mice. At different injection times (0, 1, 3, 6, 12, and 24 h) the mice were anesthetized and subsequently scanned using a small animal PA imaging system (λ_{ex} = 808 nm; pulse duration: 5 − 10 ns; frequency rate: 20 Hz).

Analysis of biodistribution and pharmacokinetics about Ru-$Ti_3C_2T_x$-PEG. When the mice tumor volume was greater than 60 mm^3, Ru-$Ti_3C_2T_x$-PEG (10 mg kg^{-1}, 100 μL) was administrated into CT26

tumor-bearing mice intravenously. After different time intervals (1, 3, 6, 12, and 24 h), the tumors and main organs of various groups were obtained after killing the mice. These tissues were weighed and dissolved in a mixture of HNO_3 and HCl. Then, the clarified solution was obtained and analyzed the concentration of Ti in different tissues was analyzed by ICP-OES. The biodistribution curve of Ru-$Ti_3C_2T_x$-PEG in the body at different times. For the pharmacokinetics investigation, the mice were treated with Ru-$Ti_3C_2T_x$-PEG (100 μL, 10 mg kg^{-1}) intravenously. Taking a certain amount of blood (10 μL) from the tail vein of mice at various injection times (0, 5, 10, 20, 30 min, 1, 2, 4, 8, 12, and 24 h), and then added into physiological saline (990 μL). Afterwards, the Ti content of each sample was analyzed by ICP-OES. Using a double-compartment pharmacokinetic model to determine the *in vivo* circulating half-life ($\tau_{1/2}$) of Ru-$Ti_3C_2T_x$-PEG in the bloodstream. The eliminating rate curve was generated by plotting Ln (C_p) against time, with the data fitting according to the two-compartment models.

***In vivo* photothermal imaging.** PBS, $Ti_3C_2T_x$-PEG, and Ru-$Ti_3C_2T_x$-PEG (10 mg kg^{-1}, 100 μL) were injected into CT26 tumor-bearing mice intravenously. The mice were anesthetized by using isoflurane after 6 h of administration, and the 808 nm laser was fixed and irradiated the central part of the tumor. Using an infrared thermal imager to measure thermal images and temperature changes every 60 s.

Mild hyperthermia-enhanced cancer nanocatalytic therapy. Thirty CT26 tumor-bearing mice were randomly divided into six groups, including G1: Control, G2: Laser, G3: $Ti_3C_2T_x$-PEG, G4: Ru-$Ti_3C_2T_x$-PEG, G5: $Ti_3C_2T_x$-PEG + Laser, G6: Ru-$Ti_3C_2T_x$-PEG + Laser (the tumor sites were irradiated with 808 nm laser for 5 min after 6 h of injection). The $Ti_3C_2T_x$-PEG and Ru-$Ti_3C_2T_x$-PEG were administrated with the dose of 10 mg kg^{-1} at days 1, 4, 7, 10, and 13, respectively. The tumor size and body weight of mice in all treatment groups were measured every 2 days, and the tumor volume was calculated as follows: $V = L \times W^2 /2$, where L and W represent the length (mm) and width (mm), respectively. The mice were sacrificed on

day 15 and the tumor weight was recorded. For histopathological analysis, the main organ and tumor tissue sections of representative mice in each experimental group were collected and stained with hematoxylin eosin (H&E), the stained sections were observed and analyzed by using the Leica TCS SP8 instrument. Also, the tumor tissues were also stained with TdT-mediated dUTP nick end labeling (TUNEL) for detecting apoptotic cells.

Animal experiments. The female BALB/c mice (4-week-old) were purchased from Beijing Vital River Laboratory Animal Technology Co., Ltd. (Beijing, China) (1100111084356). The procedure of animal experiments conformed to the Guidelines for Care and Use of Laboratory Animals of the Drug Safety Evaluation Center of Harbin Medical University. And the Animal experiments were approved by the Ethics Committee of the Second Affiliated Hospital of Harbin Medical University (No. GZRDW 2022-001). CT26 cells (1×10^6, 100 μL in PBS) were subcutaneously injected into the right hind limb of each BALB/c mouse aged 5 weeks to establish CT26 tumor models, and the following experiments were conducted when the tumor volume approached 50 mm^3.

Statistical analysis. All the quantitative data were presented as mean ± S.D. And statistical differences were calculated by using an unpaired two-tailed Student's *t*-test with GraphPad Prism 9.0 (GraphPad Software, Inc, CA, USA). The significance levels were denoted as $^{**}p < 0.01$ (moderately significant) and $^{***}p < 0.001$ (highly significant).

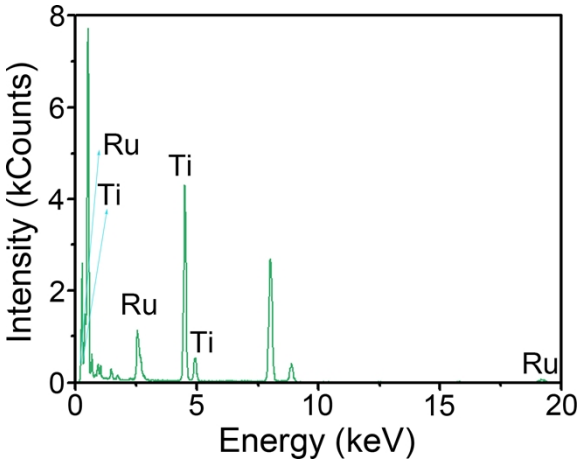

Fig. S1. Energy dispersive X-ray spectrum of Ru-$Ti_3C_2T_x$.

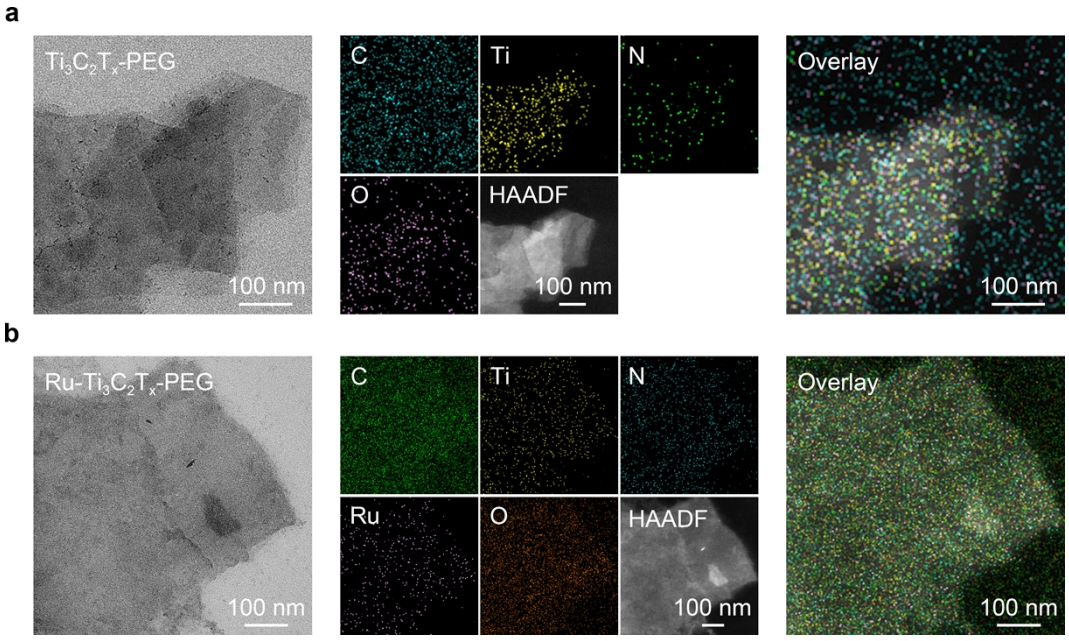

Fig. S2. TEM, HAADF-STEM, and the corresponding elemental mapping images of (a) $Ti_3C_2T_x$-PEG and (b) Ru-$Ti_3C_2T_x$-PEG nanozymes.

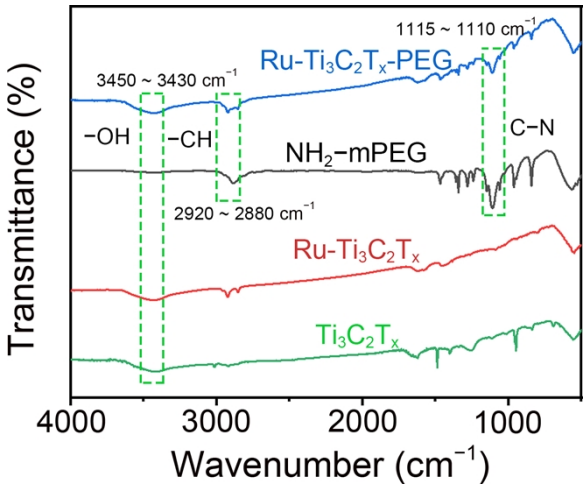

Fig. S3. FTIR spectra of $Ti_3C_2T_x$, Ru-$Ti_3C_2T_x$, Ru-$Ti_3C_2T_x$-PEG, and NH_2-mPEG, respectively.

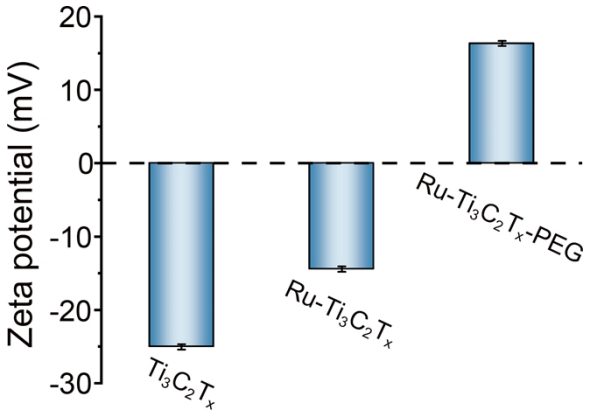

Fig. S4. The Zeta potentials of different samples during the synthesis process.

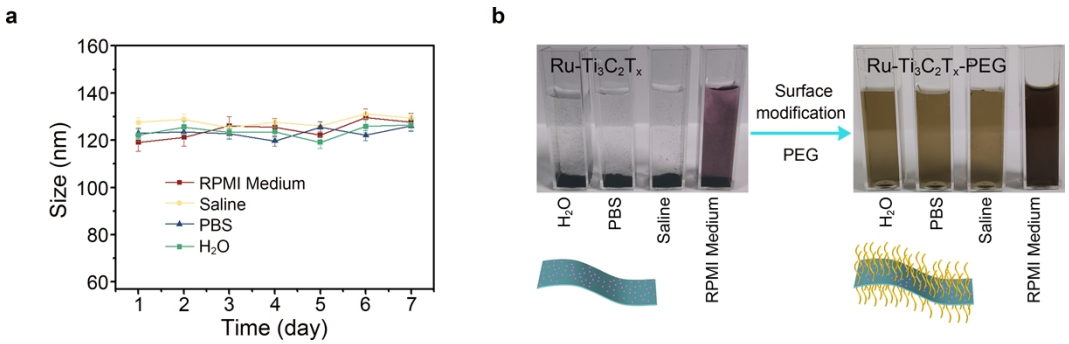

Fig. S5. (a) Hydrodynamic dimension changes of Ru-$Ti_3C_2T_x$-PEG nanocomposites dispersed in different physiological solutions for different incubation times. (b) Digital images of Ru-$Ti_3C_2T_x$ and Ru-$Ti_3C_2T_x$-PEG dispersed in different physiological solutions.

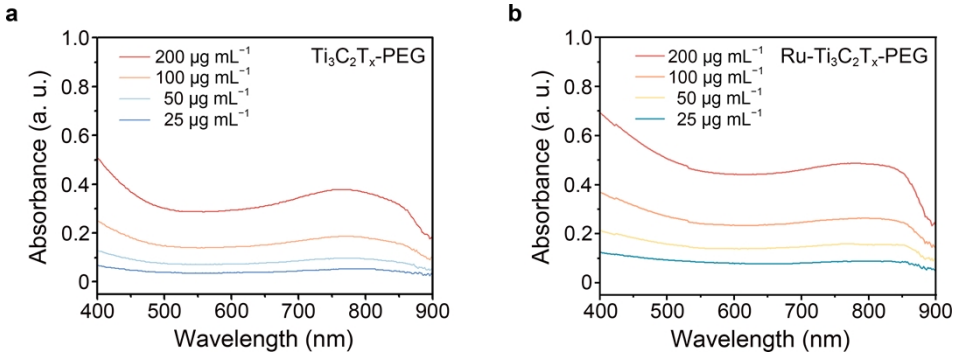

Fig. S6. The UV−vis absorption spectra of (a) $Ti_3C_2T_x$-PEG and (b) Ru-$Ti_3C_2T_x$-PEG nanocatalysts with different concentrations.

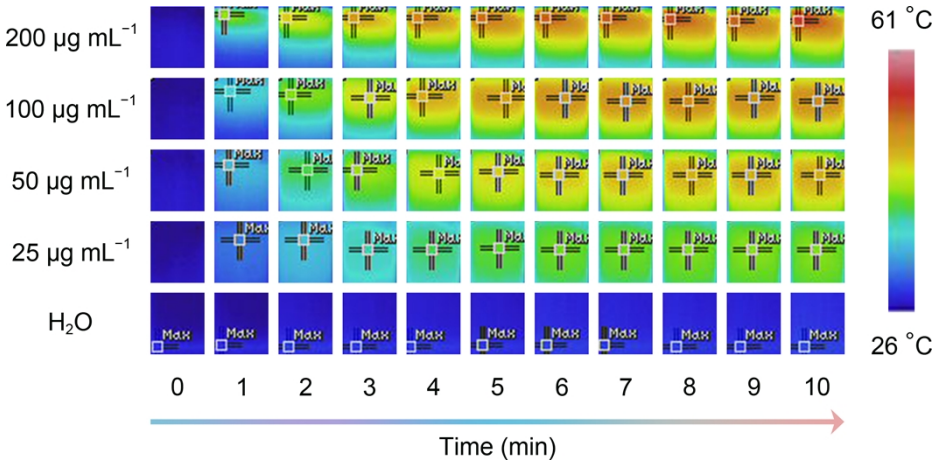

Fig. S7. Digital photographs of Ru-$Ti_3C_2T_x$-PEG with different concentrations irradiated upon 808 nm laser.

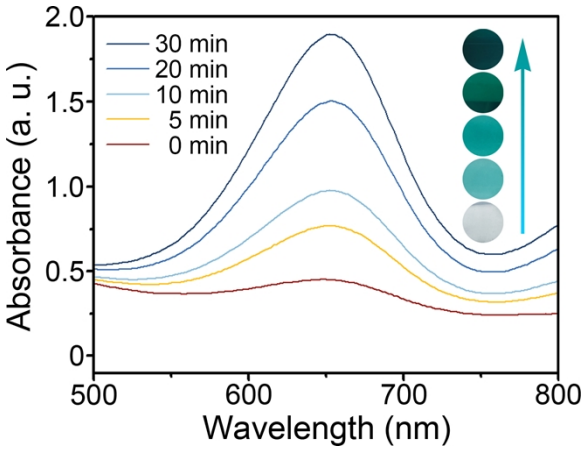

Fig. S8. UV−vis absorption spectra of the oxTMB catalyzed by Ru-$Ti_3C_2T_x$-PEG *versus* different reaction times, inset showed the corresponding digital photographs of sample color change in each group.

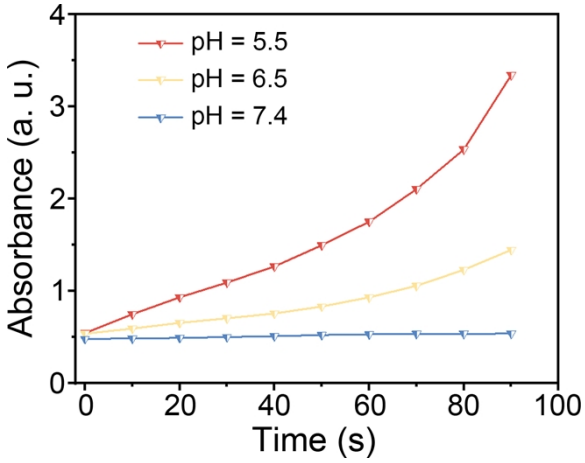

Fig. S9. UV−vis absorption spectra of the oxTMB catalyzed by Ru-$Ti_3C_2T_x$-PEG dispersed in PBS with different pH values.

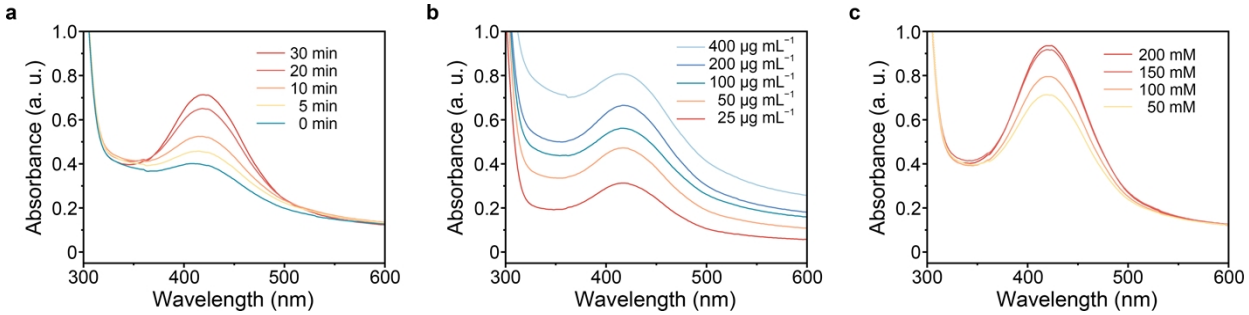

Fig. S10. (a) UV−vis absorption spectra of the oxidized OPD catalyzed by Ru-$Ti_3C_2T_x$-PEG (200 μg mL^{-1}) *versus* reaction time. (b) The UV−vis absorption spectra of the oxidized OPD with the addition of Ru-$Ti_3C_2T_x$-PEG at different concentrations. (c) The UV−vis absorption spectra of the oxidized OPD in the presence of Ru-$Ti_3C_2T_x$-PEG (200 μg mL^{-1}) and H_2O_2 with different concentrations.

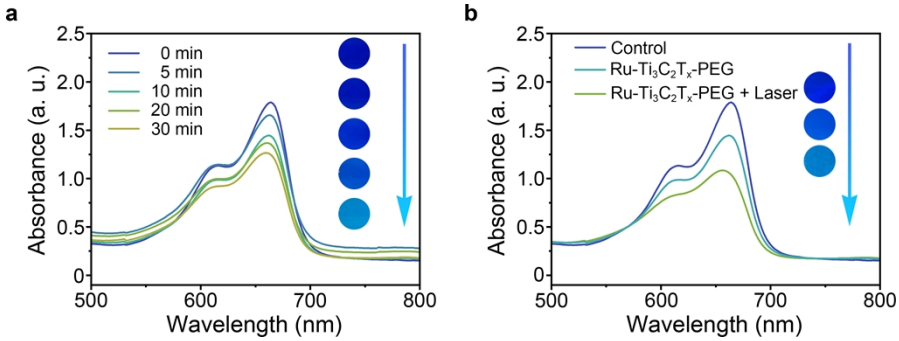

Fig. S11. (a) UV−vis absorption spectra of the oxidized MB catalyzed by Ru-$Ti_3C_2T_x$-PEG *versus* different reaction times. (b) The UV−vis absorption spectra of the oxidized MB by Ru-$Ti_3C_2T_x$-PEG for 10 min irradiated with or without 808 nm laser.

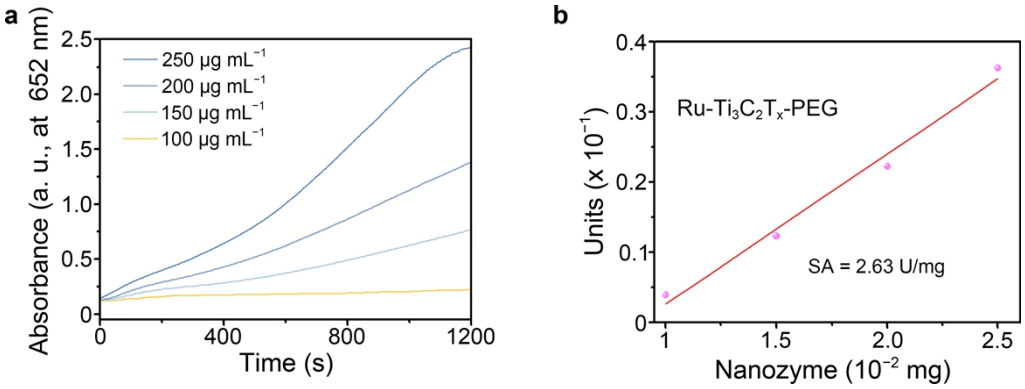

Fig. S12. (a) The initial linear portion of the reaction-time curves of Ru-$Ti_3C_2T_x$-PEG with different concentrations. (b) The specific nanozyme activity of Ru-$Ti_3C_2T_x$-PEG.

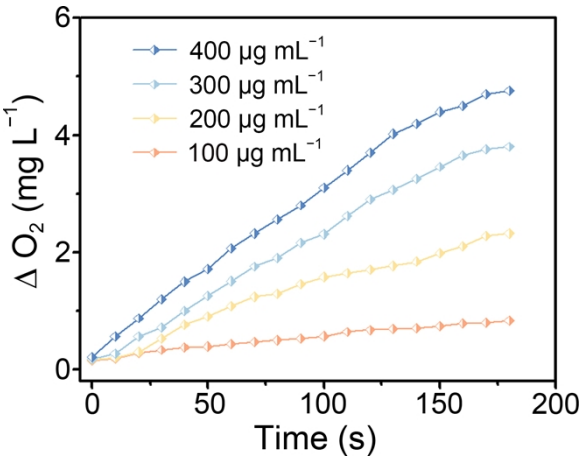

Fig. S13. Oxygen generation by Ru-$Ti_3C_2T_x$-PEG at different concentrations *versus* reaction time with the addition of H_2O_2.

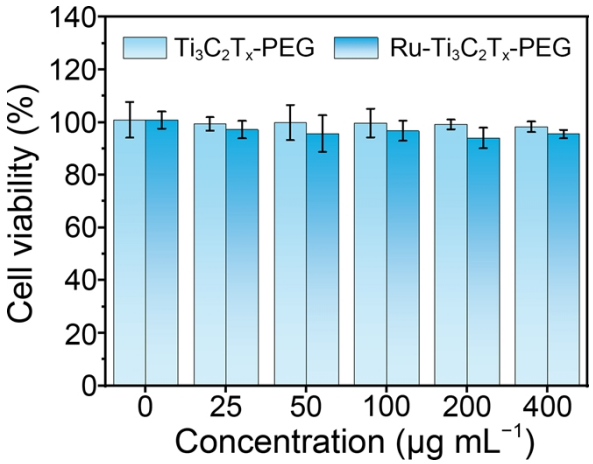

Fig. S14. Relative cell viabilities of L929 cells incubated with $Ti_3C_2T_x$-PEG and Ru-$Ti_3C_2T_x$-PEG at different concentrations for 24 h.

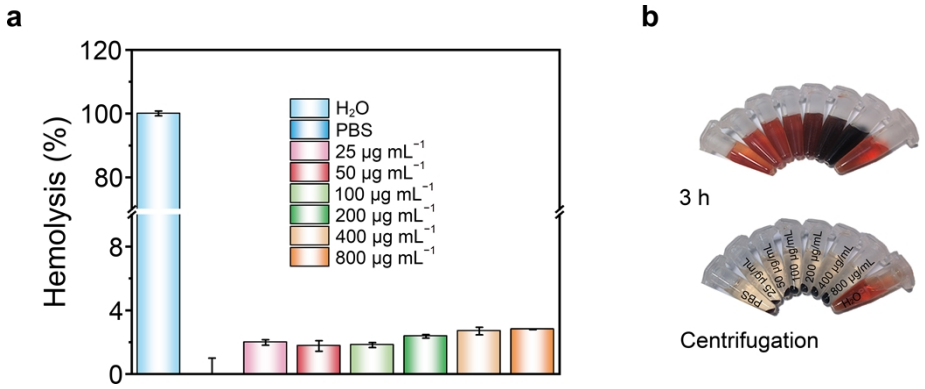

Fig. S15. (a) Hemolysis analysis of blood incubated with water (positive control), PBS (negative control), and Ru-$Ti_3C_2T_x$-PEG at different concentrations. (b) The corresponding digital photograph of different samples by centrifugation after 3 h of incubation.

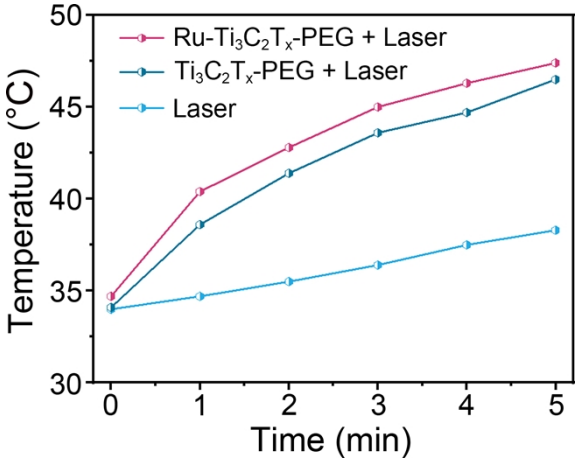

Fig. S16. Temperature change curves corresponding to *in vivo* photothermal imaging of tumor-bearing mice after different treatments.

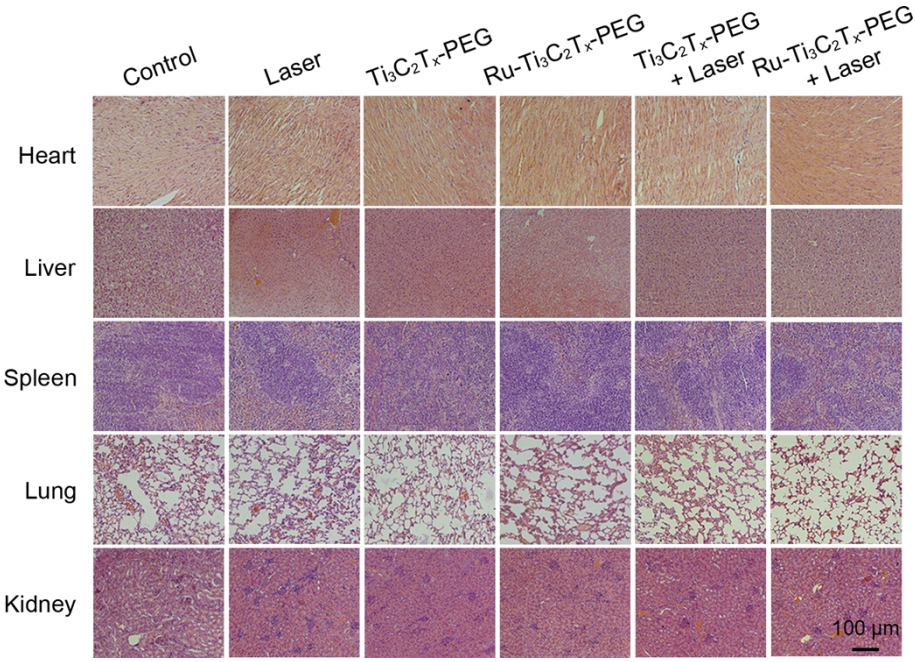

Fig. S17. H&E-stained images of heart, liver, spleen, lung, and kidney obtained from representative mice in different groups after 15 days of treatment.